nature medicine

Brief Communication

https://doi.org/10.1038/s41591-023-02475-5

A reinforcement learning model for AI-based decision support in skin cancer

Received: 31 August 2022

Accepted: 28 June 2023

Published online: 27 July 2023

Check for updates

Catarina Barata[1,16], Veronica Rotemberg[2,16], Noel C. F. Codella[3], Philipp Tschandl[4], Christoph Rinner[5], Bengu Nisa Akay[6], Zoe Apalla[7], Giuseppe Argenziano[8], Allan Halpern[2], Aimilios Lallas[7], Caterina Longo[9,10], Josep Malvehy[11,12], Susana Puig[11,12], Cliff Rosendahl[13], H. Peter Soyer[14], Iris Zalaudek[15] & Harald Kittler[4]

We investigated whether human preferences hold the potential to improve diagnostic artificial intelligence (AI)-based decision support using skin cancer diagnosis as a use case. We utilized nonuniform rewards and penalties based on expert-generated tables, balancing the benefits and harms of various diagnostic errors, which were applied using reinforcement learning. Compared with supervised learning, the reinforcement learning model improved the sensitivity for melanoma from 61.4% to 79.5% (95% confidence interval (CI): 73.5–85.6%) and for basal cell carcinoma from 79.4% to 87.1% (95% CI: 80.3–93.9%). AI overconfidence was also reduced while simultaneously maintaining accuracy. Reinforcement learning increased the rate of correct diagnoses made by dermatologists by 12.0% (95% CI: 8.8–15.1%) and improved the rate of optimal management decisions from 57.4% to 65.3% (95% CI: 61.7–68.9%). We further demonstrated that the reward-adjusted reinforcement learning model and a threshold-based model outperformed naïve supervised learning in various clinical scenarios. Our findings suggest the potential for incorporating human preferences into image-based diagnostic algorithms.

Compared to clinical experts, artificial intelligence (AI)-based diagnostic methods have demonstrated similar or better accuracy in various areas of diagnostic imaging. As a result, AI-based decision-support tools are expected to facilitate access to expert-level image-based diagnostic accuracy[1–6]. To ensure the safety and effectiveness of AI-enabled medical devices, certain performance quality standards must be met. For example, regulations governing cancer diagnosis emphasize high sensitivity due to the greater potential harm of overlooking a malignancy compared to misclassifying a benign lesion as malignant. However, evaluating a diagnostic test based solely on sensitivity is

[1]Institute for Systems and Robotics, LARSyS, Instituto Superior Técnico, Lisbon, Portugal. [2]Dermatology Service, Memorial Sloan Kettering Cancer Center, New York, NY, USA. [3]Microsoft, Redmond, WA, USA. [4]Department of Dermatology, Medical University of Vienna, Vienna, Austria. [5]Center for Medical Statistics, Informatics and Intelligent Systems (CeMSIIS), Medical University of Vienna, Vienna, Austria. [6]Ankara University School of Medicine, Department of Dermatology, Ankara, Turkey. [7]Second Department of Dermatology, Aristotle University of Thessaloniki, Thessaloniki, Greece. [8]Dermatology Unit, University of Campania, Naples, Italy. [9]Dermatology Unit, University of Modena and Reggio Emilia, Modena, Italy. [10]Azienda Unità Sanitaria Locale – IRCCS di Reggio Emilia, Centro Oncologico ad Alta Tecnologia Diagnostica-Dermatologia, Reggio Emilia, Italy. [11]Melanoma Unit, Dermatology Department, Hospital Clínic Barcelona, Universitat de Barcelona, IDIBAPS, Barcelona, Spain. [12]Centro de Investigación Biomédica en Red de Enfermedades Raras (CIBER ER), Instituto de Salud Carlos III, Barcelona, Spain. [13]General Practice Clinical Unit, Medical School, The University of Queensland, Brisbane, Queensland, Australia. [14]Frazer Institute, The University of Queensland, Dermatology Research Centre, Brisbane, Queensland, Australia. [15]Department of Dermatology, Medical University of Trieste, Trieste, Italy. [16]These authors contributed equally: Catarina Barata, Veronica Rotemberg. e-mail: harald.kittler@meduniwien.ac.at

https://doi.org/10.1038/s41591-023-02475-5

a

	MEL	BCC	AKIEC	BKL	NV	DF	VASC
MEL	5	−3	−4	−5	−5	−5	−5
BCC	−2	3	−2	−4	−4	−4	−4
AKIEC	−2	−2	2	−3	−3	−3	−3
BKL	−3	−2	−2	1	−2	−2	−2
NV	−3	−2	−2	−2	1	−2	−2
DF	−3	−2	−2	−2	−2	1	−2
VASC	−3	−2	−2	−2	−2	−2	1

b

	MEL	BCC	AKIEC	BKL	NV	DF	VASC
MEL	0.61	0.02	0.05	0.08	0.22	0.01	0.01
BCC	0.04	0.80	0.06	0.06	0.02	0.01	0.00
AKIEC	0.00	0.09	0.81	0.05	0.05	0.00	0.00
BKL	0.05	0.02	0.05	0.81	0.06	0.01	0.00
NV	0.06	0.02	0.01	0.07	0.84	0.00	0.00
DF	0.00	0.05	0.05	0.05	0.11	0.75	0.00
VASC	0.00	0.03	0.00	0.00	0.09	0.06	0.83

c

	MEL	BCC	AKIEC	BKL	NV	DF	VASC
MEL	0.80	0.03	0.01	0.05	0.09	0.01	0.01
BCC	0.03	0.87	0.03	0.03	0.02	0.01	0.00
AKIEC	0.07	0.12	0.77	0.05	0.00	0.00	0.00
BKL	0.11	0.06	0.03	0.76	0.03	0.02	0.00
NV	0.13	0.02	0.01	0.06	0.77	0.00	0.00
DF	0.00	0.05	0.05	0.05	0.11	0.75	0.00
VASC	0.00	0.06	0.00	0.00	0.06	0.06	0.83

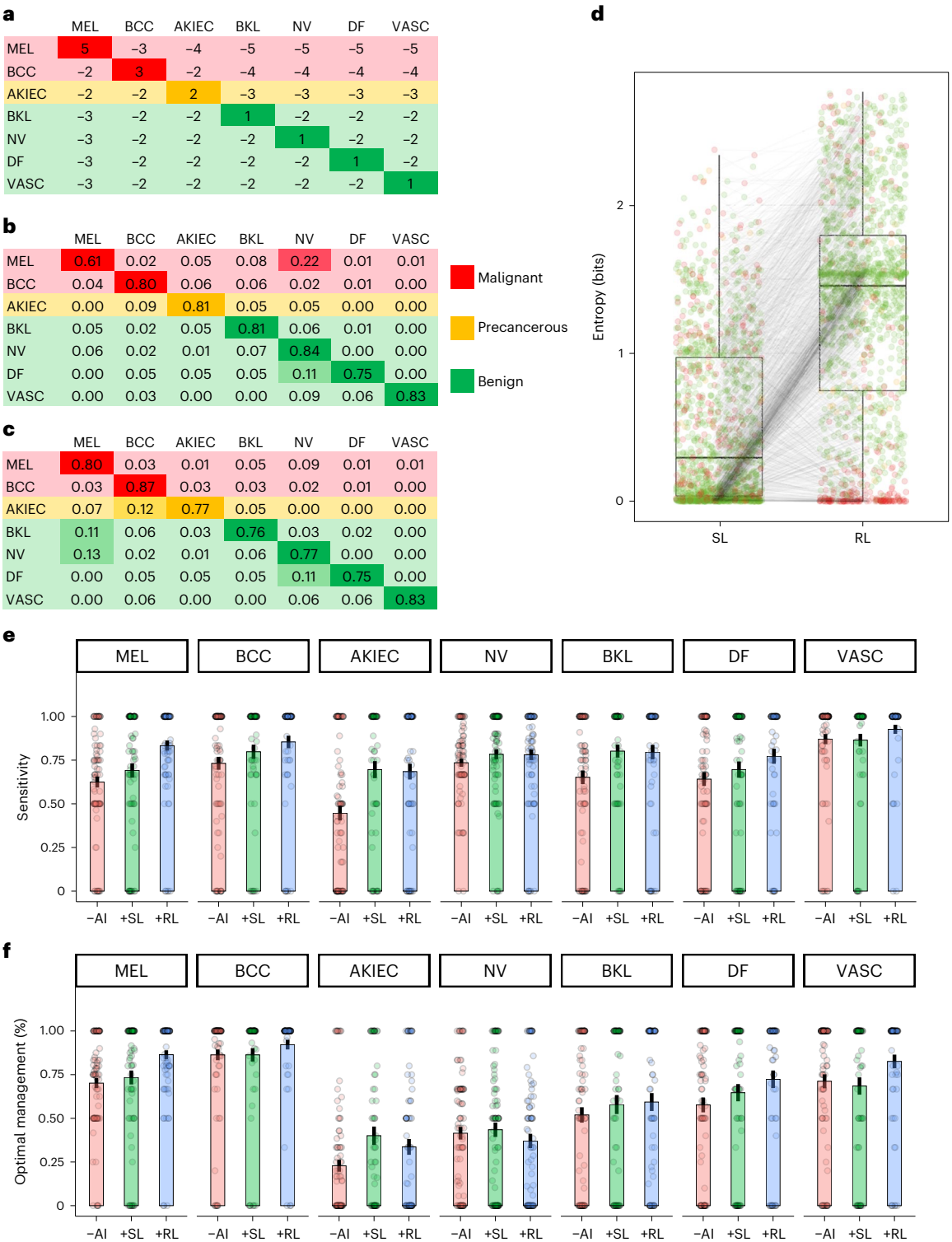

Fig. 1 | Comparison of models and reader study results. a, Expert-generated reward table used to train the RL model; rows, ground truth; columns, predictions. **b**,**c**, Confusion matrix of the SL model (**b**) and the RL model (**c**) using the same test set ($n = 1511$). Rows, ground truth; columns, predictions. The proportions are normalized by the row-sums (MEL: $n = 171$; BCC: $n = 93$; AKIEC: $n = 43$; BKL: $n = 217$; NV: $n = 908$; DF: $n = 44$; VASC: $n = 35$). **d**, Boxplot of difference in entropy of paired test set predictions ($n = 1,511$) of the SL model and the RL model. Black line, median; boxes, 25th–75th percentiles; whiskers, minimum and maximum values, $P < 0.0001$ (Wilcoxon test). **e**,**f**, Results of the reader study comparing sensitivities (**e**) and frequencies of optimal management decisions (**f**) of 89 dermatologists by diagnosis without AI support (−AI), with support by the SL model (+SL) and with support by the RL model (+RL). Optimal managements: 'excision' for melanomas and basal cell carcinomas; 'local therapy' for actinic keratoses/intraepidermal carcinoma; and 'dismiss' for nevi, benign keratinocytic lesions, dermatofibroma and vascular lesions. Bars, means; whiskers, standard error. Sample sizes: MEL(−AI): $n = 89$; MEL(+SL): $n = 78$; MEL(+RL): $n = 81$; BCC(−AI): $n = 89$; BCC(+SL): $n = 63$; BCC(+RL): $n = 68$; AKIEC(−AI): $n = 89$; AKIEC(+SL): $n = 60$; AKIEC(+RL): $n = 72$; NV(−AI): n = 89; NV(+SL): $n = 88$; NV(+RL): $n = 85$; BKL(−AI): $n = 89$; BKL(+SL): $n = 65$; BKL(+RL): $n = 76$; DF(−AI): $n = 89$; DF(+SL): $n = 71$; DF(+RL): $n = 61$; VASC(−AI): $n = 89$, VASC(+SL): $n = 67$; VASC(+RL): $n = 65$. Abbreviations: MEL, melanoma; BCC, basal cell carcinoma; AKIEC, actinic keratosis/intraepidermal carcinoma; BKL, benign keratinocytic lesion; NV, melanocytic nevus; DF, dermatofibroma; VASC, vascular lesion.

inadequate as low specificity also poses risks, such as invasive procedures, patient anxiety and waste of healthcare resources. The trade-off between these harms differs depending on the type of cancer and is further influenced by human preferences, which refers to the personal judgments of physicians and patients regarding the relative value of potential outcomes within a specific clinical scenario. These preferences are not usually taken into account in AI training, but at best are implemented at more application-level logic through thresholds and cost-sensitive learning[7–9].

Diagnostic procedures can be viewed as a sequential decision-making task in which a management decision is based on the likelihood of a potentially harmful diagnosis like cancer. In the field of diagnostic imaging, we can think of this as a Markov decision process where the initial states are image attributes, the possible actions are management strategies and the rewards are determined by the relative benefits and harms of diagnostic errors and appropriate and inappropriate management decisions. In this way, we can use reinforcement learning to find a strategy that maximizes cumulative rewards while considering clinician and patient preferences[10,11].

To test whether reinforcement learning could be useful to adapt AI predictions to human preferences, we used the example of skin cancer diagnosis. This domain is challenging for AI because it involves imbalanced datasets dominated by benign conditions and represents a multiclass problem involving more than one type of cancer with different trade-offs[12]. Although less common than other skin cancers, melanoma has the highest mortality rate, and overlooking melanoma should carry a higher penalty than overlooking other types of skin cancer[13].

First, we trained a supervised learning model (SL model) using a publicly available training set composed of 10,015 images including two types of skin cancer, melanoma and basal cell carcinoma, a precancerous condition (actinic keratosis/intraepidermal carcinoma) and four common benign conditions (nevi, benign keratinocytic lesions, dermatofibroma and vascular lesions)[14]. The model was trained to minimize a class-frequency weighted cross-entropy loss, with the goal to maximize average recall. The output of the model predicted multiclass probabilities for each of the seven diagnoses. The external validity of this model was tested on an independent test set of 1,511 images, where the model achieved an average accuracy of 77.8% with a sensitivity of 61.4% for melanoma (95% CI: 54.1–68.7%) and 79.6% for basal cell carcinoma (95% CI: 71.4–87.8%). This result is comparable to the results of above-average models obtained in an international competition using the same benchmark test set, and better than the results obtained by experts[3]. Although the model has acceptable multiclass accuracy, the low sensitivity for melanoma limits its use in clinical practice.

Next, we set up a reinforcement learning model (RL model) with deep *Q*-learning using a one-dimensional vector combining the multiclass probabilities and the feature vector of the SL model as the initial state[11]. We used a dermatologist-generated reward table in which rewards and penalties for correct and incorrect diagnoses depend on the type of skin cancer (Fig. 1a). Using the same training and test sets, the RL model achieved a significantly higher sensitivity for melanoma (79.5%, 95% CI: 73.5–85.6%, $P < 0.001$) and for basal cell carcinoma (87.1%, 95% CI: 80.3–93.9%, $P < 0.001$) compared to the baseline SL model while maintaining a high average accuracy of 79.2% (Fig. 1b,c). This increase in sensitivity for melanoma was mainly driven by reclassifying melanomas diagnosed as nevi by the SL model (Extended Data Fig. 1a).

We also calculated the Shannon entropy of AI predictions and used it as a marker of model uncertainty. We found that the RL model increased the entropy of predictions in comparison to the SL model (median: 0.30 bits, 25th–75th percentile: 0.04–0.97 bits versus median: 1.46 bits, 25th–75th percentile: 0.75–1.80 bits, $P < 0.001$; Fig. 1d). While this increase in uncertainty has no decremental effect on average accuracy, it reduces the overconfidence of AI predictions when the diagnosis is incorrect (median: 1.13 bits, 25th–75th percentile: 0.82–1.49 bits for 298 cases incorrectly classified by the SL model versus 1.81 bits, 25th–75th percentile: 0.90–2.32 bits for 333 cases incorrectly classified by the RL model, $P < 0.001$). While the addition of human preferences increased the uncertainty of predictions on average, it decreased the uncertainty for melanomas if they were correctly predicted by the RL model (Fig. 1d and Extended Data Fig. 1b).

Next, we investigated the utility of the RL model for management decisions in a human-in-the-loop scenario. We conducted a reader study with 89 dermatologists who had to diagnose the same image with and without AI support and determine management, choosing between four treatment decisions: dismiss, excise, treat locally or monitor. For AI support, dermatologists were alternately offered the multiclass probabilities of the SL or the RL model. The rate of correct diagnoses increased from 68.0% (95% CI: 65.3–70.6%) without AI support to 75.3% with SL model support (mean difference +7.3%, 95% CI: 4.6–10.2%, $P < 0.001$) and to 79.9% with RL model support (mean difference +12.0%, 95% CI: 8.8–15.1%, $P < 0.001$). The readers' sensitivity for melanoma improved from 62.4% (95% CI: 56.3–68.6.0%) without support to 69.4% (95% CI: 61.3–77.0%, $P < 0.001$) with SL model support and to 83.9% (95% CI: 77.7–89.0%, $P < 0.001$) with RL model support. The sensitivity for basal cell carcinoma was similarly improved while the sensitivity for other diagnoses did not decrease substantially (Fig. 1e). Furthermore, management decisions of expert readers improved with AI support (Fig. 1f). The proportions of optimal management decisions increased from 57.4% (95% CI: 54.2–60.5%) without AI support to 61.7 (95% CI: 58.0–65.3%, $P = 0.03$) with SL model support and to 65.3% (95% CI: 61.7–68.9%, $P < 0.001$) with RL model support. This improvement was most pronounced for melanoma (without AI: mean = 70.1%, 95% CI: 64.5–75.7%; SL model support: mean = 73.4%, 95% CI: 65.5–81.2%, $P = 0.51$, and RL model support: mean = 86.4%, 95% CI: 81.5–91.4%, $P < 0.001$).

Finally, we compared the reward-based RL model with a threshold-based SL model and a naïve model that simply chooses the optimal management strategy according to the top 1 class prediction of the SL model. To this end, we created three different clinical scenarios and used thresholds and rewards provided by ten experts in the field of skin cancer diagnosis (Fig. 2).

For the simplest scenario, we divided the data into a malignant (melanoma, basal cell carcinoma, actinic keratosis/intraepidermal carcinoma) and a benign class (nevi, vascular lesions, dermatofibroma

Fig. 2 | Comparison of models in three different scenarios. Top level (binary scenario: benign versus malignant): **a**, Experts' malignancy probability thresholds for decision to excise ($n = 10$). Lines, median; boxes, 25th–75th percentiles; whiskers, values within 1.5 times interquartile range. **b**, Receiver operating characteristic curve derived from the SL model and operating points of ten experts using either thresholds (SL model) or rewards (RL model). Possible management decisions were 'dismiss' or 'excise'. True and false positive rates refer to proportions of malignant and benign lesions that were excised. Black triangle, naïve approach (excision if malignant probability > 0.5). **c**, Boxplot comparing TPRs for melanomas applying thresholds (SL model) and rewards (RL model) provided by ten experts. Bars, means; whiskers, standard deviations ($P = 0.11$, paired *t*-test); dashed line, naïve approach. Middle level (multiclass scenario, additional therapeutic option): **d**, Thresholds of ten experts for probabilities of actinic keratosis/intraepidermal carcinoma for decision to treat locally. Line, median; boxes, 25th–75th percentiles; whiskers, values within 1.5 times interquartile range. **e**, Median rewards per action and diagnosis. **f**–**h**, Confusion matrices of actions by diagnosis: naïve approach (**f**), threshold-adjusted SL model (**g**) and RL model (**h**). Lower level (patient-centered approach, 7,375 lesions, 524 patients): **i**, Thresholds of ten experts for malignancy probabilities for decision to dismiss, monitor or excise. **j**, Median rewards per action and diagnosis. **k**, Number of excisions of benign lesions by patient according to model. **l**, Number of monitored benign lesions by patient according to model. **m**, Management strategies for 55 melanomas according to model.

https://doi.org/10.1038/s41591-023-02475-5

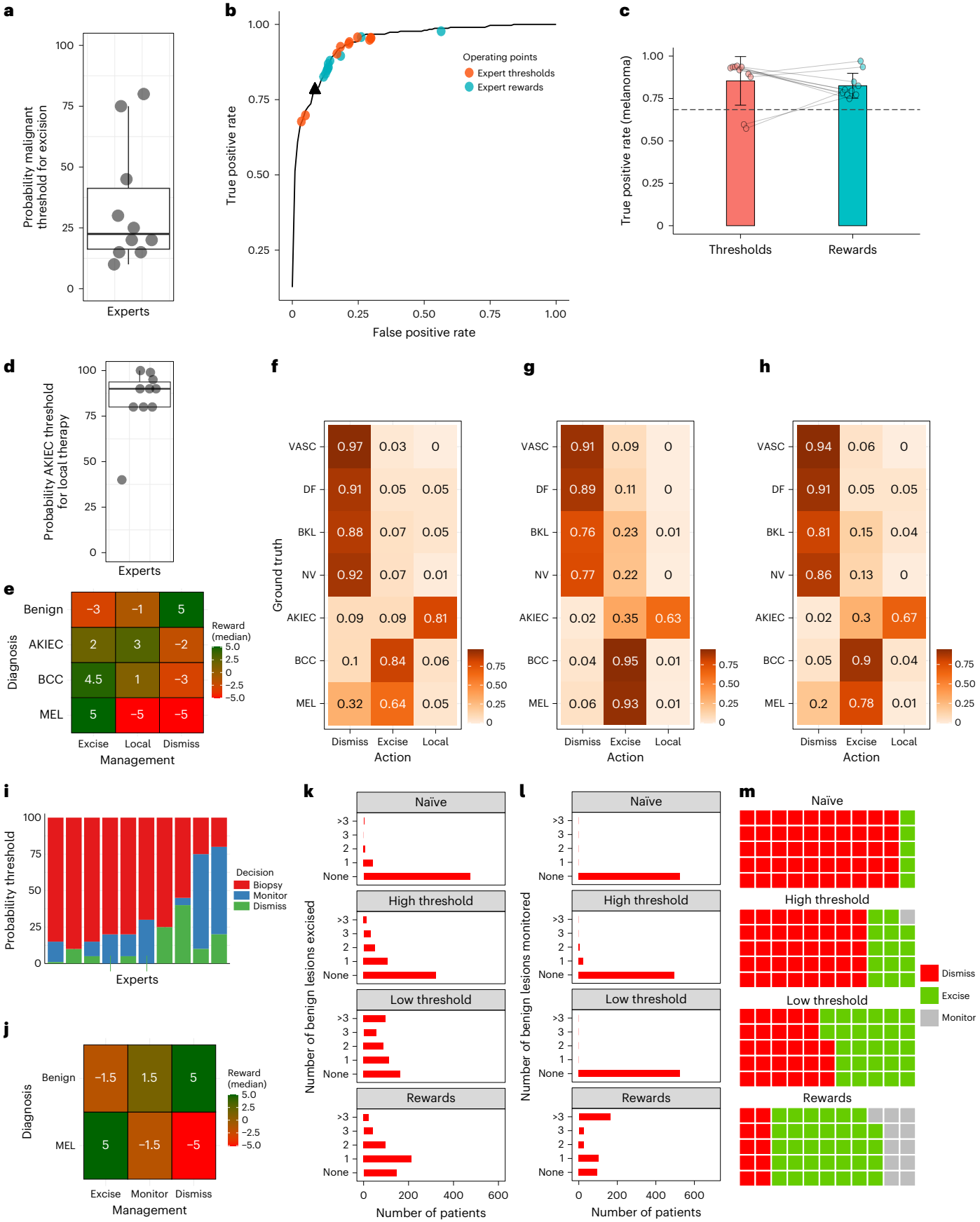

and benign keratinocytic lesions) and considered only two treatment options, either 'dismiss' or 'excision'. In this scenario, the proportion of malignant lesions that were managed by excision represented the true positive rate (TPR). As shown in Fig. 2b, the threshold-adjusted SL model and the reward-based RL model caused a shift in operating points on the receiver operating curve, bringing them closer to regions with an increased TPR. While the TPR was 78.2% for the naïve approach, it increased to 88.9% (95% CI: 80.9–96.9%) for the threshold-adjusted SL model and to 88.0% (95% CI: 83.4–92.5%) for the RL model. As shown in Fig. 2c, the TPR for melanoma was 68.4% for the naïve approach, 85.4% (95% CI: 74.7–96.0%) for the threshold-adjusted SL model and 82.5% (95% CI: 75.7–89.3%) for the RL model. The difference between the two models was not significant ($P = 0.11$).

In a second scenario, we explored all seven diagnoses and added local therapy as a treatment option. While excision is the optimal management for melanoma and most basal cell carcinomas, local therapy is optimal for actinic keratosis/intraepidermal carcinoma. For this scenario, we used the median values of the expert estimates for both rewards and thresholds. We found that the threshold- and reward-based model were superior to the naïve model in increasing the frequency of the optimal management decision as well as in preventing mismanagement of malignant lesions (Fig. 2c–e and Extended Data Fig. 2). In the 307 malignant conditions that require treatment, mismanagement was at 21.8% in the naïve approach (95% CI: 17.2–26.4%), 13.4% in the RL model (95% CI: 9.8–17.7%) and 5.2% in the threshold-adjusted SL model (95% CI: 3.0–8.3%, $P < 0.0001$).

The most complex scenario involved monitoring of high-risk individuals with multiple nevi. Nevi are not only indicators of melanoma risk but also are potential precursors or may have morphologic criteria similar to melanoma. Most melanomas detected during monitoring are noninvasive, slow-growing lesions that mimic nevi. Short-term monitoring of these melanomas, while not optimal, is considered acceptable, as reflected in the moderate penalty set by the experts for this procedure (Fig. 2j). Because this scenario requires a more patient-centered and less lesion-centered decision-making approach, we created an RL model in which each episode consisted of all lesion images of a single patient to maximize the cumulative reward per patient. Here, as before, we used the median values of the expert estimates, except for the low-threshold model, for which we used the minimum value. In a test set of 7,375 lesions (7,320 benign lesions (98.5% nevi) and 55 noninvasive or microinvasive melanomas) from 524 patients (median: 12 lesions per patient, range: 6–51), the naïve approach would remove 9.1% ($n = 5$) of melanomas, while two patients (0.4%) would have >3 benign lesions removed. The threshold approach would remove 25.5% ($n = 14$) of melanomas and >3 benign lesions in 13 patients (2.4%). As shown in Fig. 2k, lowering the threshold results in a high number of patients with >3 excised benign lesions ($n = 98$, 18.6%) and with an increase of excised melanomas (49.1%, $n = 27$). The RL model would remove 61.8% ($n = 34$) and monitor 20% ($n = 11$) of melanomas, outperforming all other models in terms of acceptable management decisions for these melanomas (Extended Data Fig. 3). At the same time, 23 patients (4.4%) would have >3 benign lesions removed. A distinctive feature of the RL model would be the high number of benign lesions (41.6%, $n = 3{,}045$) that are monitored (Fig. 2f–h). This strategy aligns with the practices of expert clinicians when monitoring high-risk patients, aiming at reducing the number of missed melanomas while keeping the number of excisions within an acceptable range.

Here, we demonstrate that the integration of human preferences, represented as reward tables created by experts, enhances the performance of a pretrained AI decision-support system. Improvement is evident in both the system's standalone performance and its ability to collaborate effectively with dermatologists. Dermatologists' improvement may be due to the RL model reducing AI overconfidence by considering consequences of management decisions. We further show that incorporating human preferences improves management decisions in complex clinical scenarios. This optimization of medical decision-making has traditionally been captured by risk–benefit analysis, but due to the complexity of this method, individualized medical decision-making is not yet attainable[15]. The current trend toward AI-based decision support in medicine presents an opportunity to implement individualized medical decision-making in clinical practice. However, this can only happen if the concept of incorporating human preferences is also given greater consideration in the development of such systems.

Based on our results, we suggest that RL, among other techniques, could be a suitable tool for this purpose, although it is not necessarily the best solution. A limitation of the RL method is that the model must be retrained, whereas other simpler approaches, such as thresholding, can be applied without retraining. As demonstrated in our binary scenario, both methods—that is, the threshold method and the RL method—will improve management decisions compared to the naïve SL model by optimizing operating points on a decision curve. Another limitation is that we included only physicians' but not patients' preferences. There is growing emphasis on patient-centered care, where the preferences and needs of patients are considered. For future clinical applications, we envision physicians and patients collaborating in shared medical decision-making to jointly develop reward tables. Creating reward tables would provide a secondary benefit of making rewards explicit and transparent, enhancing the acceptance of AI decision-support tools. Our study focused on management decisions related to skin cancer diagnosis. Although the basic concepts can be applied to other diagnostic scenarios, those outside diagnostic medicine may require different approaches.

In conclusion, our study shows that incorporating human preferences can improve AI-based diagnostic decision support and that such preferences could be considered when developing AI tools for clinical practice. RL could be a potential alternative to threshold-based methods for creating tailored approaches in complex clinical scenarios. However, additional research, including evaluating patient and provider satisfaction, is necessary to fully uncover the potential of RL in this context.

Online content

Any methods, additional references, Nature Portfolio reporting summaries, source data, extended data, supplementary information, acknowledgements, peer review information; details of author contributions and competing interests; and statements of data and code availability are available at https://doi.org/10.1038/s41591-023-02475-5.

References

1. Esteva, A. et al. Dermatologist-level classification of skin cancer with deep neural networks. *Nature* **542**, 115–118 (2017).
2. Tschandl, P. et al. Human-computer collaboration for skin cancer recognition. *Nat. Med.* https://doi.org/10.1038/s41591-020-0942-0 (2020).
3. Tschandl, P. et al. Comparison of the accuracy of human readers versus machine-learning algorithms for pigmented skin lesion classification: an open, web-based, international, diagnostic study. *Lancet Oncol.* **20**, 938–947 (2019).
4. Haenssle, H. A. et al. Man against machine: diagnostic performance of a deep learning convolutional neural network for dermoscopic melanoma recognition in comparison to 58 dermatologists. *Ann. Oncol.* **29**, 1836–1842 (2018).
5. McKinney, S. M. et al. International evaluation of an AI system for breast cancer screening. *Nature* **577**, 89–94 (2020).
6. Haggenmüller, S. et al. Skin cancer classification via convolutional neural networks: systematic review of studies involving human experts. *Eur. J. Cancer* **156**, 202–216 (2021).

7. Birch, J., Creel, K. A., Jha, A. K. & Plutynski, A. Clinical decisions using AI must consider patient values. *Nat. Med.* **28**, 229–232 (2022).
8. Song, C. & Li, X. Cost-Sensitive KNN algorithm for cancer prediction based on entropy analysis. *Entropy* **24**, 253 (2022).
9. Collell, G., Prelec, D. & Patil, K. R. A simple plug-in bagging ensemble based on threshold-moving for classifying binary and multiclass imbalanced data. *Neurocomputing* **275**, 330–340 (2018).
10. Yala, A. et al. Optimizing risk-based breast cancer screening policies with reinforcement learning. *Nat. Med.* **28**, 136–143 (2022).
11. Mnih, V. et al. Human-level control through deep reinforcement learning. *Nature* **518**, 529–533 (2015).
12. Combalia, M. et al. Validation of artificial intelligence prediction models for skin cancer diagnosis using dermoscopy images: the 2019 International Skin Imaging Collaboration Grand Challenge. *Lancet Digit Health* **4**, e330–e339 (2022).
13. Miller, K. D. et al. Cancer treatment and survivorship statistics, 2022. *CA Cancer J. Clin.* https://doi.org/10.3322/caac.21731 (2022).
14. Tschandl, P., Rosendahl, C. & Kittler, H. The HAM10000 dataset, a large collection of multi-source dermatoscopic images of common pigmented skin lesions. *Sci. Data* **5**, 180161 (2018).
15. Fraenkel, L. & Fried, T. R. Individualized medical decision making: necessary, achievable, but not yet attainable. *Arch Intern Med.* **170**, 566–569 (2010).

Publisher's note Springer Nature remains neutral with regard to jurisdictional claims in published maps and institutional affiliations.

Open Access This article is licensed under a Creative Commons Attribution 4.0 International License, which permits use, sharing, adaptation, distribution and reproduction in any medium or format, as long as you give appropriate credit to the original author(s) and the source, provide a link to the Creative Commons license, and indicate if changes were made. The images or other third party material in this article are included in the article's Creative Commons license, unless indicated otherwise in a credit line to the material. If material is not included in the article's Creative Commons license and your intended use is not permitted by statutory regulation or exceeds the permitted use, you will need to obtain permission directly from the copyright holder. To view a copy of this license, visit http://creativecommons.org/licenses/by/4.0/.

© The Author(s) 2023

Methods

Supervised learning and reinforcement learning

For the supervised learning, we fine-tuned a convolutional neural network for classification of seven different categories of the HAM10000 dataset, as described previously[14]. For RL, we created a deep *Q*-learning model consisting of a multilayer perceptron that receives as input a one-dimensional state vector from the feature vectors and probabilities of the supervised model. For the patient-centered scenario, we normalized the input vector to account for the context of multiple lesions (the lesion state vector was divided position-wise by the average across all lesion vectors of the same patient). Python language (v.3.8) was used to conduct all experiments. The RL models were implemented using TensorFlow v.2.8, together with a set of packages: NumPy (v.1.20.3), Scikit-Learn (v.1.1.2), pandas (v.1.3.4) and OpenAI Gym (v.0.23.1).

The RL models predict the *Q*-value for each possible action. Depending on the RL model, the action space was either selecting a diagnosis (seven actions) or selecting a management option, ranging from two actions (dismiss or excise) to four actions (dismiss, monitor, treat locally and excise), depending on the type of scenario. The RL models were trained following Mnih et al.[11] using an exploration–exploitation strategy, a replay buffer and a target *Q*-network with a lower update rate to stabilize the training process[11]. Huber loss was adopted as the loss function and the weights of the *Q*-network were updated using the Adam optimizer with a learning rate of 0.025. To improve generalization, we added dropout layers with a probability of 0.05. We tested different configurations for the *Q*-network (number and size of the hidden layers and combination of the input state), buffer size, episode length, update rates for the *Q*-network and the target model, and exploration ε. The best *Q*-network models consisted of a multilayer perceptron with a 256-unit fully connected layer with a ReLu activation that processes the features of the supervised model, followed by the concatenation of its output with the logits. The concatenation is fed to the output layer, which has the same units as the number of possible actions and a linear activation. The replay buffer size was set to 10,000 and the update rates for the *Q*- and target networks were set to 4 and 8,000 iterations, except in the patient-centered model where the updates were set to 35 and 5,800 iterations. We also ran experiments with several episode lengths, ranging from 250 to 12, except in the patient-centered model where the episodes had a varying length depending on the number of lesions per patient. We found that the episode length had a marginal effect on the performance of the RL model. In the case of the patient-centered model, we found that ordering the lesions according to malignancy probability inside the episode led to better performances. Finally, the ε was set to 0.2. We also found that modifications to the reward table resulted in only minor changes or degradation of results compared to the originally designed reward table.

We used the HAM10000 dataset to train all RL models, except in the patient-centered scenario[1]. To track the evolution of the models, we split the original HAM10000 set into a single 80/20 partition, of which the latter was used as the validation set. Because of the relatively small number of patients and the high variability in the number of lesions per patient, the patient-centered dataset was used to train and evaluate the RL model based on a 20-fold cross-validation strategy.

The reward table for the basic RL model was created in advance in consensus by three expert dermatologists (H.K., P.T., V.R.). To compare the reward model with the threshold model in different clinical scenarios, we asked 12 dermatologists with extensive experience in treating neoplastic skin lesions to provide us with their reward tables and thresholds for each scenario. Because two of the 12 experts provided incomplete information (they did not specify thresholds for either the binary scenario or the scenario with the additional treatment option), we had a total of ten expert assessments available. Treatment decisions using the threshold model followed a preference-based hierarchy. The model initially determined if the predicted melanoma probability exceeded the excision threshold. If not, it considered the overall malignancy probability and then the probabilities of basal cell carcinoma and actinic keratosis/intraepidermal carcinoma. The median values of the rewards and thresholds were used for the SL model and the RL model, respectively. For the low-threshold approach in the patient-centered scenario, we used the minimum value rather than the median value of the ten thresholds reported by the experts.

Entropy

We calculated the Shannon entropy as a measure of uncertainty in the predictions of the machine learning models using the following formula, where H is entropy, X is a discrete random variable with possible probabilities (p) ranging from p_1 to p_n, and i is an index variable:

$$H(X) = H(p_1, \ldots., p_n) = -\sum_{i=1}^{n} p_i \log 2p_i$$

Datasets

The publicly available HAM10000 dataset was used to train the SL model and the RL model[1].

The ISIC 2018 challenge test set was used as an independent test set for the reader study and for the external validation of the SL model and the RL model[3].This set includes 1,511 retrospectively collected dermatoscopic images from different sites including Austria (n = 928), Australia (n = 267), Turkey (n = 117), New Zealand (n = 87), Sweden (n = 92) and Argentina (n = 20) to ensure diversity of skin types. The mean age of patients was 50.8 years (s.d.: 17.4 years), and 46.2% of patients were female. The ground truth was routine pathology evaluation (n = 786), biology (that is, >1.5 years of sequential dermatoscopic imaging without changes; n = 458), expert consensus in inconspicuous cases that were not excised or biopsied (n = 260) and in vivo confocal images (n = 7). Fewer than ten cases with ambiguous histopathologic reports were excluded. For the patient-centered scenario, we used dermatoscopic images of 7,375 lesions from 524 patients (mean: 51.1 years, s.d.: 11.8 years, 46.6% females). Images were collected either at the University Department of Dermatology, Medical University of Vienna (n = 4,839) or at a dermatology practice in Vienna (n = 2,536). The consecutive dataset included 55 melanomas, all of which were either noninvasive (in situ) or microinvasive (<0.8 mm invasion thickness, tumor stage T1a). Most benign lesions that were selected for monitoring by the treating dermatologists were nevi (n = 7,213). The remaining benign lesions were keratinocytic lesions (n = 53), dermatofibromas (n = 31), or vascular lesions (n = 20) and other benign lesions (n = 3).

Interaction platform, raters and reader study

We used the web-based platform DermaChallenge, which was developed at the Medical University of Vienna, as the interface for the reader study[16].The platform is split into a back end and front end, and both are deployed on a stack of standard web technologies (Linux, Apache, MariaDB and PHP). The front end is optimized for mobile devices (mobile phones and tablets) but can also be used on any other platform via a JavaScript-enabled web browser. Readers were recruited by using mailing lists and social media posts from the International Society of Dermoscopy. To participate in the study, raters had to register with a username, a valid email address and a password. In addition, we asked for age (age groups spanning 10 years), sex, country and profession. The readers' task was to diagnose the unknown test images first without and then with decision support based on either the SL model or the RL model. The images were presented in batches of ten selected randomly from the test set of 1,511 images. We drew a stratified random sample to ensure a predefined class distribution of three nevi, two melanomas and one example of each other class. Readers could repeat the survey with different batches at their own discretion. The study was online from 17th November 17th 2022 to 2nd February 2023. During this time, we collected 613 complete tests from 89 dermatologists.

Statistical analysis

Comparisons of continuous data between groups were performed with paired or unpaired *t*-tests or Wilcoxon signed-rank tests, as appropriate. Chi-square tests or McNemar tests were used for proportions. Reported *P* values are two-sided and a *P* value < 0.05 was regarded as statistically significant. All analyses were performed with R Statistics v.4.2.1 (ref. 17) and plots were created with ggplot2 v.3.3.6.

Ethics statement and informed consent

This project was conducted after ethics review by the Ethics Review Board of the Medical University of Vienna (Protocol No. 1804/2017, Amendment 4th April 2022). When registering, all participants of the reader study platform agreed that their data could be used for scientific research and were made aware that they could revoke this consent at any time. Readers received no compensation for their participation.

Reporting summary

Further information on research design is available in the Nature Portfolio Reporting Summary linked to this article.

Data availability

The origin of the training set images is reported in the dataset-publication of HAM10000 in Nature Scientific Data [14]. Training set images are available from the ISIC Image Archive at https://api.isic-archive.com/collections/66/ or the Harvard Dataverse at https://doi.org/10.7910/DVN/DBW86T (ref. 18). Test set images are available from the ISIC Image Archive at https://challenge.isic-archive.com/data/#2018. The ISIC image archive initially featured a test set comprising 1,512 images, but for this research, one image known as the 'easter egg' (ISIC_0035068) was excluded. The ground truth of the test set images is available from the Harvard Dataverse at https://doi.org/10.7910/DVN/DBW86T (ref. 18). Anonymous reader data of the test set images and the entire image dataset used in the patient-centered model can be downloaded from the Harvard Dataverse at https://doi.org/10.7910/DVN/PWQMQ7 (ref. 19).

Code availability

The code for the supervised learning model is available athttps://github.com/ptschandl/dermatoscopy_resnet34_nmed_2020. The code for the reinforcement learning model is available at https://github.com/catarina-barata/Skin_RL.

References

16. Rinner, C., Kittler, H., Rosendahl, C. & Tschandl, P. Analysis of collective human intelligence for diagnosis of pigmented skin lesions harnessed by gamification via a web-based training platform: simulation reader study. *J. Med. Internet Res.* **22**, e15597 (2020).
17. R Core Team. *R: A Language and Environment for Statistical Computing* (R Foundation for Statistical Computing, 2022).
18. Tschandl, P. The HAM10000 dataset, a large collection of multi-source dermatoscopic images of common pigmented skin lesions. Harvard Dataverse, V4 https://doi.org/10.7910/DVN/DBW86T(2018).
19. Harald, K. A reinforcement learning model for AI based decision support in skin cancer. Harvard Dataverse https://doi.org/10.7910/DVN/PWQMQ7(2023).

Acknowledgements

C.B. was partially funded by the FCT project and multiyear funding (CEECIND/ 00326/2017) and LARSyS - FCT Plurianual funding 2020–2023. V.R. was funded by MSK Cancer Center Support Grant/Core Grant (P30 CA008748) and NIH/NCI U24 CA264369-01. The funders had no role in the study design, data collection and analysis, decision to publish or preparation of the manuscript. We would like to thank all dermatologists who participated in the online reader study for their important contributions.

Author contributions

C.B., V.R. and H.K. initiated this work. C.B. and H.K. supervised the study and C.B., V.R., H.K., N.C.F.C. and A.H. drafted the manuscript. P.T., B.N.A., Z.A., G.A., A.H., A.L., C.L., J.M., S.P., C.R., H.P.S. and I.Z. collected data for the reader study, P.T., C.R. and H.K. created the reader study platform and designed the reader study. P.T., C.R. and H.K., collected images for the training and test sets and C.B., P.T. and H.K conducted the statistical analysis and had direct access to and verified the data reported in the manuscript. All authors contributed to finalizing the manuscript and reviewed the final version. C.B. and V.R. are equal contributors listed as first coauthors, H.K. is the senior and corresponding author.

Competing interests

The authors declare the following competing interests: P.T. has received fees from Silverchair, speaker honoraria from FotoFinder, Lilly and Novartis, and an unrestricted one-year postdoc grant from MetaOptima Technology Inc. N.C. is a Microsoft employee and owns diverse investments across technology and healthcare companies. A.H. is a consultant to Canfield Scientific Inc. and advisory board member of Scibase AB. H.P.S. is a shareholder of MoleMap NZ Limited and e-derm consult GmbH and undertakes regular teledermatological reporting for both companies. H.P.S. is also a medical consultant for Canfield Scientific Inc., MoleMap Australia Pty Ltd, Blaze Bioscience Inc. and a medical adviser for First Derm. V.R. is a medical adviser for Inhabit Brands, Inc. H.K. received nonfinancial support from Derma Medical Systems, Fotofinder and Heine, and speaker fees from Fotofinder. The remaining authors declare no competing interests.

Additional information

Extended data is available for this paper at https://doi.org/10.1038/s41591-023-02475-5.

Supplementary information The online version contains supplementary material available at https://doi.org/10.1038/s41591-023-02475-5.

Correspondence and requests for materials should be addressed to Harald Kittler.

Peer review information *Nature Medicine* thanks Olivier Gevaert, Adam Yala and Matthew S. Brown for their contribution to the peer review of this work. Primary Handling Editor: Ming Yang, in collaboration with the *Nature Medicine* team.

Reprints and permissions information is available at www.nature.com/reprints.

https://doi.org/10.1038/s41591-023-02475-5

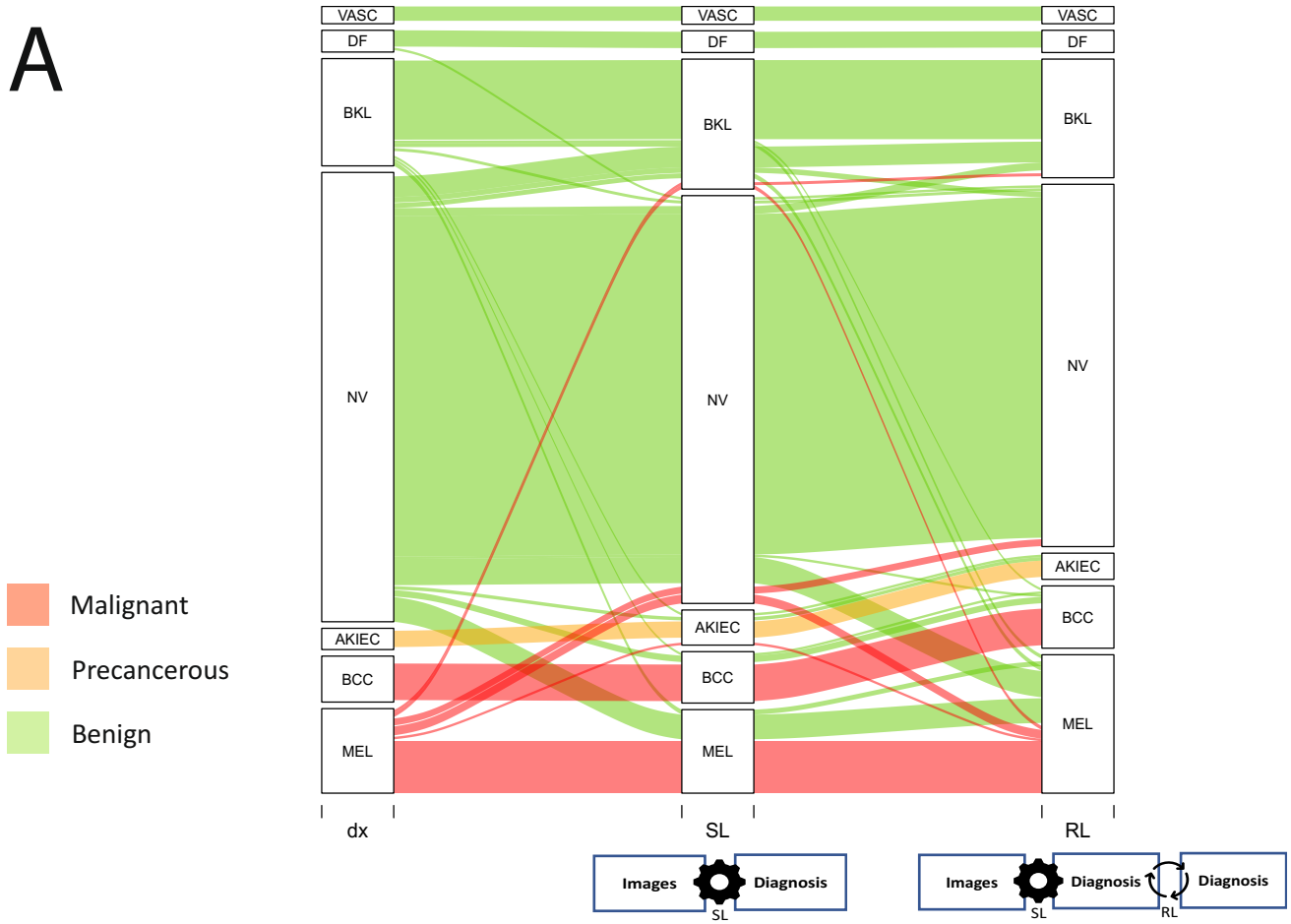

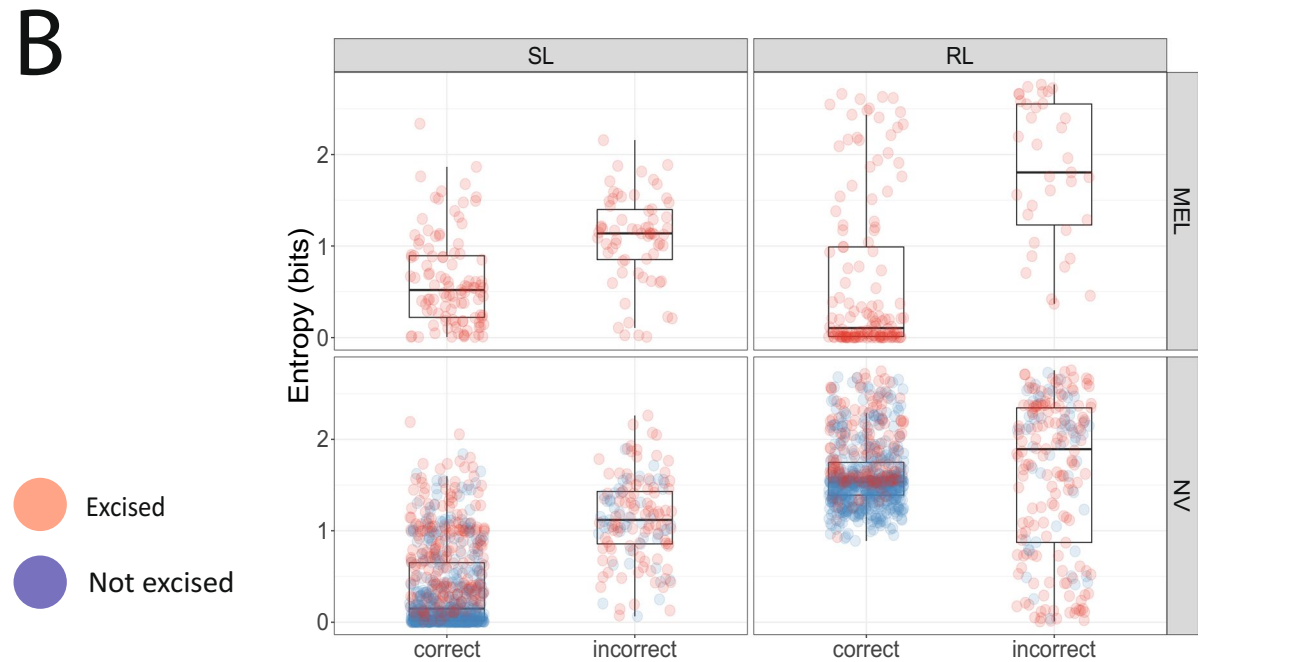

Extended Data Fig. 1 | Comparison of baseline SL model with RL model. **a**: Alluvial plot of test set (n = 1511); the left block shows the ground truth, the middle block shows the results of supervised learning (SL), and the right block shows the results of reinforcement learning (RL) based on a reward table created by experts; Only alluvials with n > 5 are shown. MEL= melanoma (n = 171), BCC= basal cell carcinoma (n = 93), AKIEC= actinic keratosis and intraepidermal carcinoma(n = 43), BKL= benign keratinocytic lesion (n = 217), NV= melanocytic nevus (n = 908), DF=dermatofibroma (n = 44), VASC= vascular lesion (n = 35). **b**: Boxplots of entropy of correct and incorrect predictions for melanoma (n = 171) and melanocytic nevi (n = 908) according to applied model. Black line = median, boxes = 25th–75th percentiles, whiskers = values within 1.5 times interquartile range; Abbreviations: SL= supervised learning, RL= reinforcement learning, dx =ground truth.

https://doi.org/10.1038/s41591-023-02475-5

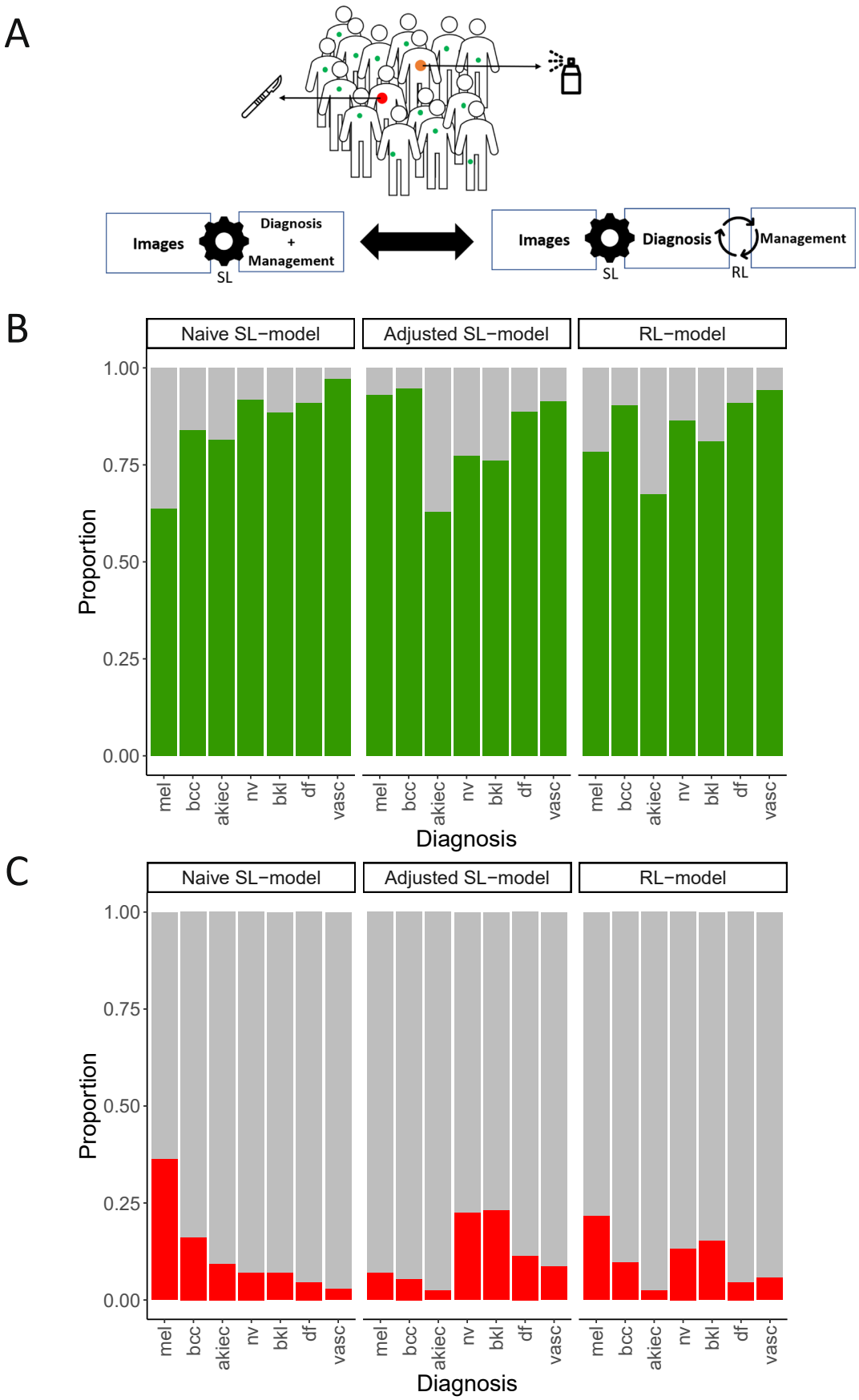

Extended Data Fig. 2 | See next page for caption.

https://doi.org/10.1038/s41591-023-02475-5

Extended Data Fig. 2 | Scenario with 7 diagnoses and 'local therapy' as an additional treatment option. a: Graphical abstract of scenario adding the treatment option 'local therapy' (for example cryotherapy) for actinic keratosis/intraepidermal carcinomas. While excision is the optimal management for melanoma and most basal cell carcinomas, local therapy is optimal for actinic keratosis/intraepidermal carcinoma. We judged local therapy to be a harmful treatment for melanomas and suboptimal for basal cell carcinomas suitable for surgery (all basal cell carcinomas in the dataset). **b**: Proportion of cases per diagnosis and model that received optimal management (excision for melanoma and basal carcinoma, local therapy for actinic keratoses/intraepidermal carcinoma, and no treatment ('dismiss') for all benign diagnoses); **c**: Proportion of cases per diagnosis and model that were mismanaged. Mismanagement included all procedures except excision for melanoma and basal cell carcinoma, all procedures except excision or local therapy for actinic keratoses/intraepidermal carcinoma, and all procedures except 'dismiss' for all benign conditions (nevus, benign keratinocytic lesions, dermatofibroma, and vascular lesions). Abbreviations and sample size: mel= melanoma (n = 171), bcc= basal cell carcinoma (n = 93), akiec= actinic keratosis/intraepidermal carcinoma(n = 43), bkl= benign keratinocytic lesion (n = 217), nv= nevus (n = 908), df=dermatofibroma (n = 44), vasc= vascular lesion (n = 35).

https://doi.org/10.1038/s41591-023-02475-5

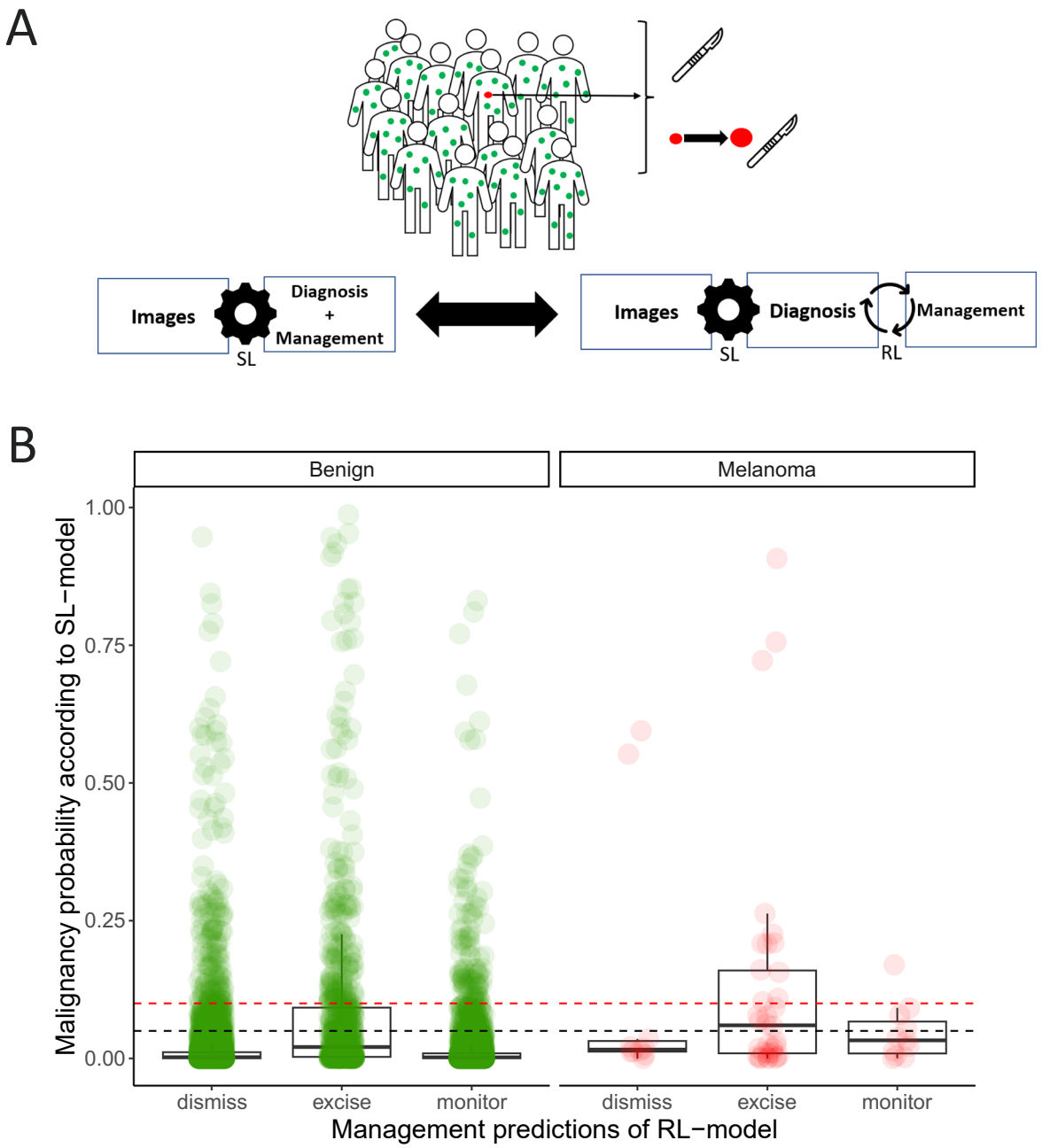

Extended Data Fig. 3 | Scenario of high-risk patients with multiple nevi. **a**: Graphical abstract of scenario of monitoring of high-risk individuals with multiple nevi. Due to the large number of lesions per patient, this scenario requires a more patient-centered and less lesion-centered approach. Most melanomas detected during monitoring are noninvasive, slow-growing lesions. Short-term monitoring of these melanomas, while not optimal, is considered acceptable. **b**: Malignancy probability predictions of the baseline SL model according to management predictions of the RL model for benign lesions (n = 7320) and melanomas (n = 55). The red dashed horizontal line indicates the median value of the melanoma probability selected by 10 experts as threshold for excision. The black dashed horizontal line indicates the minimum value. Black line = median, boxes = 25th–75th percentiles, whiskers = values within 1.5 times the interquartile range.

nature portfolio

Corresponding author(s): Harald Kittler

Last updated by author(s): Jun 19, 2023

Reporting Summary

Nature Portfolio wishes to improve the reproducibility of the work that we publish. This form provides structure for consistency and transparency in reporting. For further information on Nature Portfolio policies, see our Editorial Policies and the Editorial Policy Checklist.

Statistics

For all statistical analyses, confirm that the following items are present in the figure legend, table legend, main text, or Methods section.

n/a	Confirmed
☐	☒ The exact sample size (*n*) for each experimental group/condition, given as a discrete number and unit of measurement
☐	☒ A statement on whether measurements were taken from distinct samples or whether the same sample was measured repeatedly
☐	☒ The statistical test(s) used AND whether they are one- or two-sided *Only common tests should be described solely by name; describe more complex techniques in the Methods section.*
☐	☒ A description of all covariates tested
☐	☒ A description of any assumptions or corrections, such as tests of normality and adjustment for multiple comparisons
☐	☒ A full description of the statistical parameters including central tendency (e.g. means) or other basic estimates (e.g. regression coefficient) AND variation (e.g. standard deviation) or associated estimates of uncertainty (e.g. confidence intervals)
☐	☒ For null hypothesis testing, the test statistic (e.g. *F*, *t*, *r*) with confidence intervals, effect sizes, degrees of freedom and *P* value noted *Give P values as exact values whenever suitable.*
☒	☐ For Bayesian analysis, information on the choice of priors and Markov chain Monte Carlo settings
☒	☐ For hierarchical and complex designs, identification of the appropriate level for tests and full reporting of outcomes
☐	☒ Estimates of effect sizes (e.g. Cohen's *d*, Pearson's *r*), indicating how they were calculated

Our web collection on statistics for biologists contains articles on many of the points above.

Software and code

Policy information about availability of computer code

Data collection	Python language (version 3.8) was used to conduct all experiments. The RL models were implemented using Tensorflow 2.8, together with a set of packages: numpy (v1.20.3), scikit-learn (v1.1.2), pandas (v1.3.4), and open ai gym (v0.23.1). The supervised model was implement using PyTorch and had been previously used in publications, as reported in the "Methods" section of our submission. Data of the reader study was collected using a web-based platform using PHP (v7.1) and MariaDB (vS.5.60). The openSource PHP Framework Laravel (vS.5) and open Source JavaScript Framework ReactJS (v16.9) were used to implement the study platform. The code for supervised learning model is available at https://github.com/ptschandl/dermatoscopy_resnet34_nmed_2020. The code for the reinforcement learning model is available at https://github.com/catarina-barata/Skin_RL.
Data analysis	The results from the RL models were analyzed using standard scikit-learn (1.1.2) functions that allow the computation of evaluation metrics such as the confusion matrix, sensitivity scores, and balanced accuracy. A more detailed statistical analysis was performed using R Statistics R v4.2.1, using packages dplyr v1.0.7 for data manipulation, and epiR v2.0.39 for diagnostic values. Plots were created with ggplot2 v3.3.6.

For manuscripts utilizing custom algorithms or software that are central to the research but not yet described in published literature, software must be made available to editors and reviewers. We strongly encourage code deposition in a community repository (e.g. GitHub). See the Nature Portfolio guidelines for submitting code & software for further information.

Data

Policy information about availability of data

All manuscripts must include a data availability statement. This statement should provide the following information, where applicable:

- Accession codes, unique identifiers, or web links for publicly available datasets
- A description of any restrictions on data availability
- For clinical datasets or third party data, please ensure that the statement adheres to our policy

Origin of training set images is reported in the dataset-publication of HAM10000 in Nature Scientific Data (Tschandl, P., Rosendahl, C. & Kittler, H. The HAM10000 dataset, a large collection of multi-source dermatoscopic images of common pigmented skin lesions. Sci Data 5, 180161, 2018). Training set images are available from the ISIC Image Archive at https://api.isic-archive.com/collections/66/ or the Harvard Dataverse at https://doi.org/10.7910/DVN/DBW86T. Test set images are available from the ISIC Image Archive at https://challenge.isic-archive.com/data/#2018. The ISIC image archive initially featured a test set comprising 1512 images, but for this research, one image known as the "easter egg" (ISIC_0035068) was excluded. The ground truth of the test set images is available from the Harvard Dataverse at https://doi.org/10.7910/DVN/DBW86T. Anonymous reader data of the test set images and the entire image dataset used in the patient-centered model can be downloaded from the Harvard Dataverse at https://doi.org/10.7910/DVN/PWQMQ7.

Human research participants

Policy information about studies involving human research participants and Sex and Gender in Research.

Reporting on sex and gender	To participate in the study, raters had to register with a username, a valid e-mail address and a password. They were also asked for age (age groups of 10), biologic sex, country, and occupation. The options for sex were male, female, or other. We decided not to include the age, biologic sex, and country information in the reader description because these attributes are irrelevant to expertise.
Population characteristics	We recruited 101 dermatologists for the online reader study, of whom 89 completed at least one test round. Of the 89 readers, 52 were females. We recruited 58 dermatology residents, and 31 board certified dermatologists. Of the 89 readers, 47 were between 24-33 years old, 24 between 34-43 years, 9 between 44-53 years, 8 between 54-and 63 years, and one reader was older than 63 years. The expertise of each rater was measured by screening tests consisting of simple domain-specific tasks involving assigning cases to one of 7 possible diagnoses.
Recruitment	Mailings and social media posts of the International Dermoscopy Society were used to recruit targeted groups. The recruitment was focused on dermatologists. It is possible that recruitment of raters is influenced by self-selection bias and therefore biased towards the selection of motivated and skilled raters. Because of self selection bias, the generalisability of our results to a less motivated group of readers may be limited. When registering, all participants of the reader study platform agreed that their usage data may be used for scientific research and they can revoke this consent at any time. Readers received no compensation for their participation.
Ethics oversight	Ethics review board of the Medical University of Vienna, Protocol No. 1804/2017, Amendment April 4th, 2022

Note that full information on the approval of the study protocol must also be provided in the manuscript.

Field-specific reporting

Please select the one below that is the best fit for your research. If you are not sure, read the appropriate sections before making your selection.

☐ Life sciences ☒ Behavioural & social sciences ☐ Ecological, evolutionary & environmental sciences

For a reference copy of the document with all sections, see nature.com/documents/nr-reporting-summary-flat.pdf

Behavioural & social sciences study design

All studies must disclose on these points even when the disclosure is negative.

Study description	Quantitative experimental research data. In the online reader study the readers' tasks were to diagnose the unknown test images and to suggest a management strategy first without and then with decision support based on either the SL-model or the RL-model. The images were presented in batches of 10 images selected randomly from the test set of 1511 images.
Research sample	Participants of the reader study are users of a public open reader platform. They were recruited using mailing lists and social media posts from the International Society of Dermoscopy. The recruitment was focused on dermatologists and dermatology residents. It is possible that recruitment of raters is influenced by self-selection bias and therefore biased towards the selection of motivated and skilled raters. Because of self selection bias, the generalisability of our results to a less motivated group of readers may be limited. We recruited 101 readers for the online reader study, of whom 89 completed at least one test round. To participate in the study, raters had to register with a username, a valid email address, and a password. In addition, we asked for age (age groups spanning 10 years), sex, country and profession. Of the 89 readers, 52 were females. We recruited 58 dermatology residents, and 31 board

	certified dermatologists. Of the 89 readers, 47 were between 24-33 years old, 24 between 34-43 years, 9 between 44-53 years, 8 between 54-and 63 years, and one reader was older than 63 years. Origin of training and test set images is reported in the dataset-publication of HAM10000 in Nature Scientific Data (doi: 10.1038/sdata.2018.161) and The Lancet Oncology (doi: 10.1016/S1470-2045(19)30333-X).
Sampling strategy	Data collection for the reader study was performed prospectively. The sample of readers is a convenience sample by self-selection among suitable candidates (dermatologists). Based on findings in a previous study (doi.org/10.1038/s41591-020-0942-0) we observed an improvement of 13.5% with AI support with a standard deviation of 16,4%. Given this effect size and a power of 0.8 at a two-sided p-value <.05, more than 15 readers would need to be available for analysis (paired T-test). We finally recruited 89 raters.
Data collection	Data was recorded in a web-based training and study platform hosted by the Medical University of Vienna. The researchers were not present during interaction experiments, as raters could participate on any device (including smartphones, tablets, laptops and desktop computers) with internet connection and a JavaScript-enabled browser. The data collected from each reader included age, sex, country, and profession. Each rater had to perform multiple screening tests to ensure that the self-reported experience matched actual skills. During the experiments the readers' task was to diagnose the unknown test images first without and then with decision support based on either the SL-model or the RL-model. We collected the given diagnosis (single choice from 7 possible diagnoses), the selected management (single choice from 4 possible actions), and the time needed with and without AI-support.
Timing	The reader study was online from November 17th, 2022, to February 2nd, 2023, without any gaps
Data exclusions	We excluded incomplete tests.
Non-participation	Of 101 readers who started the reader study, 12 did not complete a single test and gave no reasons for non-participation
Randomization	Participants were not allocated into experimental groups. For each experiment, images were randomly selected as described in the Methods section

Reporting for specific materials, systems and methods

We require information from authors about some types of materials, experimental systems and methods used in many studies. Here, indicate whether each material, system or method listed is relevant to your study. If you are not sure if a list item applies to your research, read the appropriate section before selecting a response.

Materials & experimental systems

n/a	Involved in the study
☒	☐ Antibodies
☒	☐ Eukaryotic cell lines
☒	☐ Palaeontology and archaeology
☒	☐ Animals and other organisms
☒	☐ Clinical data
☒	☐ Dual use research of concern

Methods

n/a	Involved in the study
☒	☐ ChIP-seq
☒	☐ Flow cytometry
☒	☐ MRI-based neuroimaging